Pulmonary Pathology of End-Stage COVID-19 Disease in Explanted Lungs and Outcomes After Lung Transplantation

Abdallah Flaifel, MD,[1]* Benjamin Kwok, MD,[2]* Jane Ko, MD,[3]
Stephanie Chang, MD,[4,▫] Deane Smith, MD,[4] Fang Zhou, MD,[1,▫]
Luis A. Chiriboga, PhD,[1,▫] Briana Zeck,[1] Neil Theise, MD,[1]
Darya Rudym, MD,[2] Melissa Lesko, MD,[2] Luis Angel, MD,[2]
Andre Moreira, MD,[1] and Navneet Narula, MD[1]

From the Departments of [1]Pathology, [2]Medicine, [3]Radiology, and [4]Cardiothoracic Surgery, NYU Langone Medical Center, New York University School of Medicine, New York, NY, USA.

This article is available for CME credit. Go to academic.oup.com/ajcp/pages/journal_cme see the latest articles. The complete catalog of journal CME courses can be found at store.ascp.org.

ABSTRACT

Objectives: Patients with severe acute respiratory syndrome coronavirus 2 (SARS-CoV-2) infection may develop end-stage lung disease requiring lung transplantation. We report the clinical course, pulmonary pathology with radiographic correlation, and outcomes after lung transplantation in three patients who developed chronic respiratory failure due to postacute sequelae of SARS-CoV-2 infection.

Methods: A retrospective histologic evaluation of explanted lungs due to coronavirus disease 2019 was performed.

Results: None of the patients had known prior pulmonary disease. The major pathologic findings in the lung explants were proliferative and fibrotic phases of diffuse alveolar damage, interstitial capillary neoangiogenesis, and mononuclear inflammation, specifically macrophages, with varying numbers of T and B lymphocytes. The fibrosis varied from early collagen deposition to more pronounced interstitial collagen deposition; however, pulmonary remodeling with honeycomb change was not present. Other findings included peribronchiolar metaplasia, microvascular thrombosis, recanalized thrombi in muscular arteries, and pleural adhesions. No patients had either recurrence of SARS-CoV-2 infection or allograft rejection following transplant at this time.

Conclusions: The major pathologic findings in the lung explants of patients with SARS-CoV-2 infection suggest ongoing fibrosis, prominent macrophage infiltration, neoangiogenesis, and microvascular thrombosis. Characterization of pathologic findings could help develop novel management strategies.

INTRODUCTION

Progressive respiratory failure remains an important cause of mortality in individuals with severe acute respiratory syndrome coronavirus 2 (SARS-CoV-2) infection.[1] Many patients with coronavirus disease 2019 (COVID-19) lung disease develop acute respiratory distress syndrome (ARDS) requiring mechanical ventilation, with reported mortality rates of up to 40%.[2,3] In a subset of patients recovered from COVID-19 infection, lung function does not fully recover, and these patients may

benefit from lung transplantation in end-stage lung disease.[4] There are still no validated, evidence-based guidelines to support informed decision making for who should be considered a candidate for lung transplant.[5-7] Although pathologic characterization of postmortem lung specimens from patients who died early after COVID-19 has been extensively reported,[8-12] little is reported on the pathology of the lungs in patients who survived the acute illness and developed chronic hypoxic respiratory failure necessitating lung transplantation. Diffuse pulmonary fibrosis with focal microscopic honeycomb change has been described in two of the three antemortem specimens from patients requiring extracorporeal membrane oxygenation (ECMO) for severe COVID-19, one of whom was from a patient who underwent bilateral lung transplantation.[8] Herein, we report the pathologic changes seen in three lung explants from patients with chronic hypoxic respiratory failure due to postacute sequelae of SARS-CoV-2 infection and clinical outcomes after lung transplantation.

CASES

Patient 1

Pretransplant Clinical Course

A 40-year-old woman TABLE 1 with obesity, type 2 diabetes mellitus, hypertension, hyperlipidemia, hypothyroidism, and

latent *Mycobacterium tuberculosis* infection previously treated in 2018 was admitted to an outside hospital in mid-April 2020 for severe hypoxemic respiratory failure due to COVID-19 infection. She received hydroxychloroquine, convalescent plasma, tocilizumab, remdesivir, glucocorticoids, and empiric therapeutic anticoagulation as COVID-19–directed therapies. She also received multiple courses of antibiotics for presumed bacterial pneumonias, although her cultures remained negative.

She was never placed on invasive mechanical ventilation. Repeat nasopharyngeal SARS-CoV-2 polymerase chain reaction (PCR) became negative on hospital day 39. Her hospital course was complicated by a spontaneous right tension pneumothorax. She underwent bilateral lung transplantation 8 months after her initial presentation with COVID-19 pneumonia. Intraoperatively, the left lung had minimal chest wall adhesions; the right lung had significant dense circumferential adhesions to the chest wall, mediastinum, and diaphragm.

Posttransplant Clinical Course

The patient was extubated on postoperative day (POD) 2 and discharged on POD 13. Three weeks after her transplantation, she was able to ambulate 450 feet and climb up seven steps independently, as well as maintain oxygen saturations above 95% on room air. The

Variable	Patient 1	Patient 2	Patient 3
TABLE 1 Demographics of Patients Included in the Study			
Age, y	40	33	47
Sex	F	M	M
BMI (at time of transplant), kg/m^2	28.8	23	22.3
Comorbidities	Obesity, type 2 diabetes mellitus, hypertension, hyperlipidemia, hypothyroidism	None	None
Presenting symptoms related to COVID-19 infection	Shortness of breath, cough	Fevers, shortness of breath, cough	Fevers, shortness of breath, cough
Type of ventilatory/oxygenation support at time of transplant	High-flow nasal cannula	Venovenous ECMO	High-flow nasal cannula
Time spent on above support prior to transplant, mo	8	9	5
Complications of COVID-19 (prior to transplant)	Pneumothoraces	Pneumothoraces	Pneumothoraces with persistent bronchopleural fistulas, hydropneumothoraces, and hemothorax
	Presumed bacterial pneumonias (culture negative)	Acute limb ischemia due to spontaneous hematoma	
		Nosocomial infections (*Serratia marcescens*, *Klebsiella pneumoniae*, and *Pseudomonas aeruginosa* bacteremia)	Nosocomial infections (*P aeruginosa* and *K pneumoniae* bacteremia; *Chryseobacterium indologenes* VAP; *Candida krusei/glabrata* candidemia)
Time between diagnosis and first negative SARS-CoV-2 PCR test, d	38	Unknown	71
Time between onset of COVID-19 symptoms and transplant, mo	8	9	11
ICU stay posttransplant, d	11	37	4
Posttransplant venovenous ECMO, h	0	81	4
Posttransplant ventilator, d	2	25	1.7 (41 hours)
Pleural drainage, d	10	8	7

BMI, body mass index; COVID-19, coronavirus disease 2019; ECMO, extracorporeal membrane oxygenation; ICU, intensive care unit; PCR, polymerase chain reaction; SARS-CoV-2, severe acute respiratory syndrome coronavirus 2; VAP, ventilator-associated pneumonia.

patient has not had either recurrence of SARS-CoV-2 infection or allograft rejection following transplant at this time.

Radiologic Findings: Pretransplant and Posttransplant

Representative radiologic findings from this patient are shown in FIGURE 1 . Chest radiograph 2 months prior to transplant FIGURE 1A demonstrates hazy and patchy opacities bilaterally with multiple round lucent areas correlating with bronchiectasis. On chest computed tomography (CT) 2 months prior to transplant FIGURE 1B-E , peripheral triangular densities containing high-attenuation calcifications and mild lateral right pleural thickening are seen in the lingula and right upper lobe when viewed in soft tissue windows FIGURE 1B . Severe varicose and cystic bronchiectasis bilaterally particularly affects the left anterior upper lobe FIGURE 1C . A background of diffuse mildly heterogeneous ground-glass opacity is present in the full extent of both lungs, intermixed with focal areas of consolidation FIGURE 1C , FIGURE 1D , and FIGURE 1E . Consolidation is present in the lower lobes containing areas of bronchiectasis FIGURE 1D . Coronal image through the mid-chest shows multiple cystic areas representing severe traction bronchiectasis bilaterally and pneumatocele formation FIGURE 1E . Four months after bilateral lung transplant, chest radiograph shows postsurgical changes and clear lungs FIGURE 1F .

Gross Findings

The right and left lungs weigh 324.5 and 442.5 g, respectively. The gross findings of the explanted lungs are shown in FIGURE 1 . The pleural surface of the right lung has significant adhesions FIGURE 1G secondary to the right tension pneumothorax, and that of the left lung has few adhesions FIGURE 1H on the diaphragmatic surface. The cut surfaces of the lungs show diffuse consolidation involving the majority of the lung parenchyma of all lobes FIGURE 1I , FIGURE 1J , and FIGURE 1K . Traction bronchiectasis and bronchiolectasis with multiple smaller cysts are present FIGURE 1J . Besides the diffuse fibrosis, the left lung also has areas of peripheral, subpleural-based, pyramidal-shaped areas of fibrosis with tan-yellow streaks, as shown in the inset FIGURE 1K , that correspond to the peripheral triangular densities with high-attenuation calcifications seen on the soft tissue windows of the CT scan FIGURE 1B .

Histologic Findings

The histologic findings in the lungs are shown in FIGURE 2 . The lung parenchyma shows overlapping stages of proliferative and fibrotic phases of diffuse alveolar damage (DAD) with focal fibrin. Honeycomb change is not present. The proliferative phase shows areas of interstitial myxoid fibrosis FIGURE 2A . The fibrotic phase shows varying degrees of collagen deposition, ranging from mild interstitial fibrosis and preserved architecture FIGURE 2B to extensive collagen deposition with residual compressed alveolar spaces and peribronchiolar metaplasia FIGURE 2C and FIGURE 2D . Prominent type 2 pneumocyte hyperplasia is present in all the phases FIGURE 2E . The lung parenchyma shows diffuse mononuclear inflammation consisting of mild interstitial T lymphocytes and scattered clusters of B lymphocytes. Numerous macrophages, specifically within the

alveoli spaces, are present FIGURE 2E . The wedge-shaped areas of consolidation in the lung seen grossly correspond to foci of loose intra-alveolar fibrosis with septal calcification FIGURE 2F . These could represent either areas of organizing pneumonia with calcification or healed infarcts. Multiple smaller cysts seen grossly correspond to pneumatoceles that are lined by macrophages FIGURE 2G . In addition to the inflammation and fibrosis, there are multiple foci of increased interstitial capillary density with occasional foci of microvascular thrombosis, megakaryocytes, and platelets in the lung parenchyma FIGURE 2H and FIGURE 2I . Focal bronchopneumonia is present. The lining epithelium of scattered small airways shows squamous metaplasia. The larger pulmonary arteries show mild intimal thickening and no evidence of thromboemboli. The medium-sized muscular arteries show medial thickening with scattered recanalized thrombi and eccentric intimal thickening.

Patient 2

Pretransplant Clinical Course

A 33-year-old man TABLE 1 with no known medical problems was admitted to an outside hospital in late April 2020 for severe hypoxemic respiratory failure due to severe COVID-19 pneumonia. He received convalescent plasma, glucocorticoids, sarilumab, and empiric therapeutic anticoagulation as COVID-19–directed therapies but continued to have worsening oxygenation. The patient was cannulated for peripheral venovenous ECMO (VV-ECMO) within 2 weeks of his hospitalization for refractory severe ARDS. The patient's hospital course was complicated by pneumothorax and multiple nosocomial infections, including *Serratia marcescens*, *Klebsiella pneumoniae*, and *Pseudomonas aeruginosa* bacteremia and ventilator-associated pneumonias (VAPs) requiring prolonged courses of antibiotics. Efforts to improve his lung function and to wean VV-ECMO support were unsuccessful. He underwent bilateral lung transplantation during his ninth month of hospitalization, after being on VV-ECMO for 259 days. Intraoperatively, significant adhesions were encountered bilaterally throughout the entire pleural space with elevated bilateral diaphragms and small fibrotic lungs.

Posttransplant Clinical Course

Posttransplant, the patient was slowly weaned off mechanical ventilation and was discharged from the hospital on POD 37. Two months posttransplant, he was able to ambulate 100 feet independently and maintain an oxygen saturation of at least 96% on room air. The patient has not had either recurrence of SARS-CoV-2 infection or allograft rejection following transplant at this time.

Radiologic Findings: Pretransplant and Posttransplant

Representative radiologic findings from this patient are shown in FIGURE 3 .

Chest radiograph 3 months prior to hospital transfer shows severe bilateral parenchymal consolidation FIGURE 3A . A chest CT examination performed FIGURE 3B 19 days later shows a large right anterior pneumothorax contiguous with lung destruction, with an undulating interface with the right middle
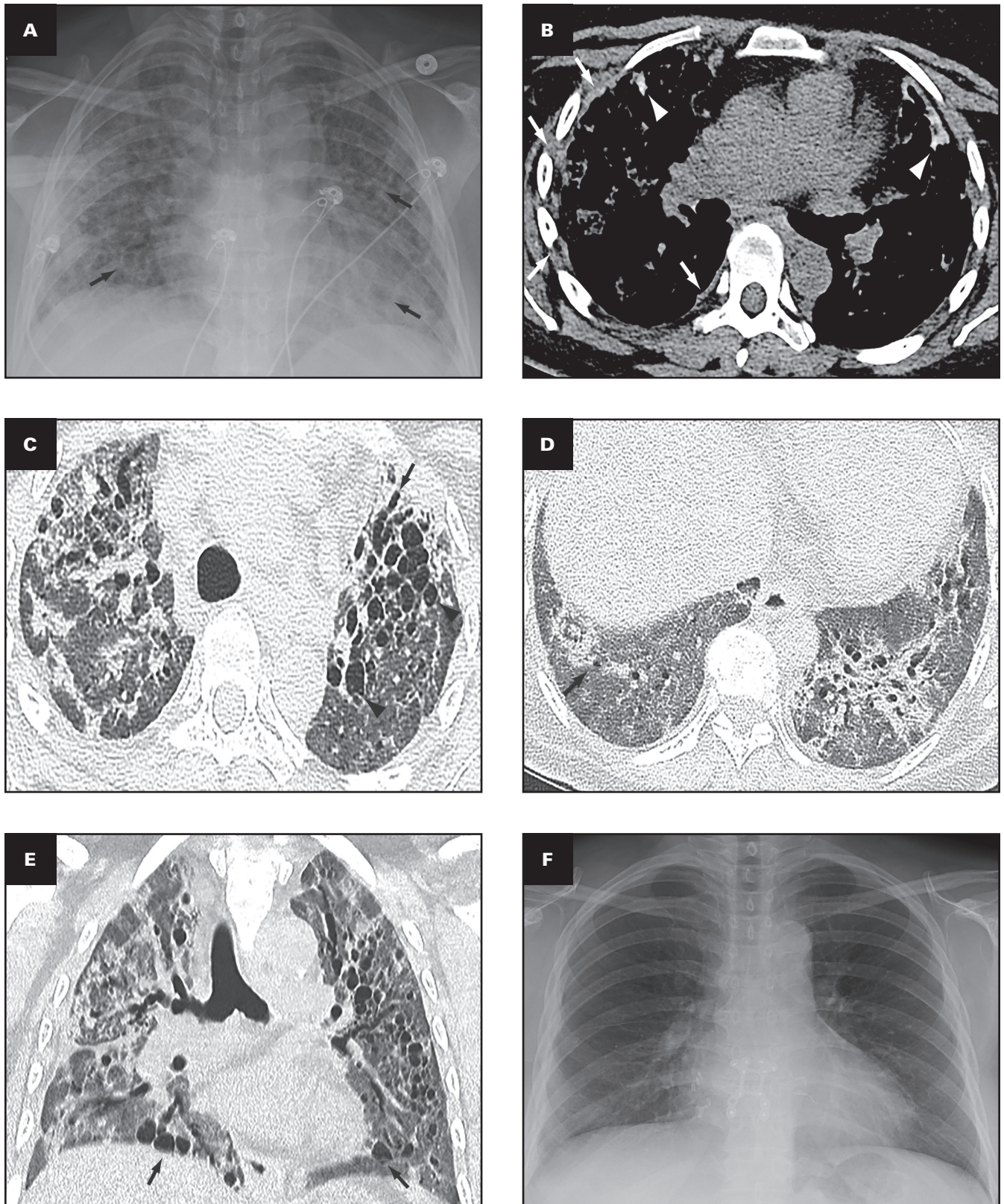
FIGURE 1 Patient 1: A 40-year-old woman with coronavirus disease 2019 prior to and after bilateral lung transplant. Overview of radiographic and gross pathologic observations. **A**, Chest radiograph 2 months prior to transplant shows lucencies representing bilateral bronchiectasis (arrows) and extensive bilateral patchy and hazy parenchymal opacities. **B**, Chest computed tomography (CT) axial soft tissue window image shows right pleural thickening (arrows) and calcified peripheral triangular densities (arrowheads). **C-E**, Chest CT lung window images show all areas of lung affected by ground-glass opacity, consolidation, and bronchiectasis. Severe bronchiectasis is present bilaterally, particularly in the upper lobes and anteriorly, such as in the left upper lobe (**C**, arrow) with cystic areas (**C**, arrowheads) that represent cystic bronchiectasis and pneumatoceles.
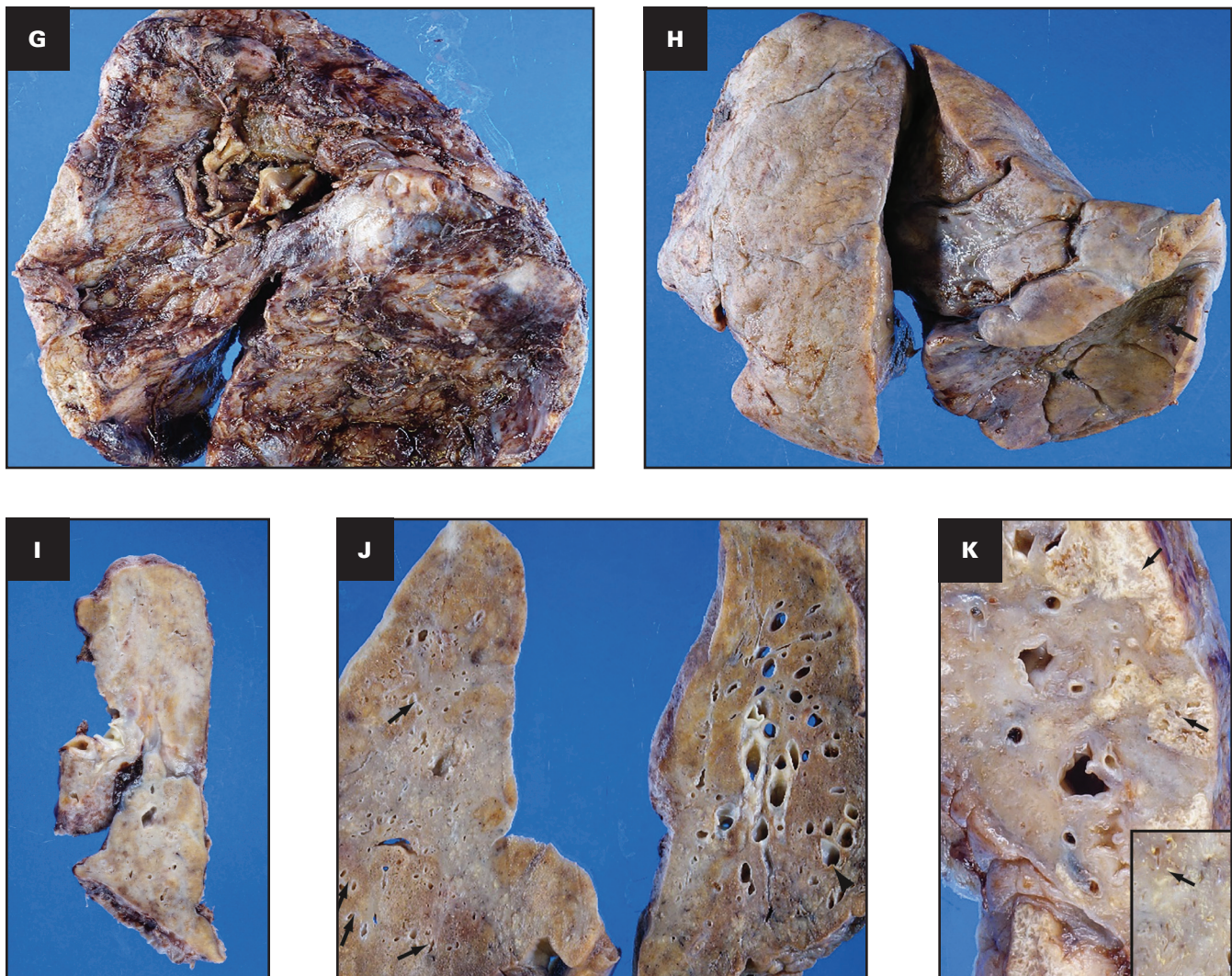
FIGURE 1 (cont) **D**, On a more caudal axial image, consolidation in the left lower lobe and right lower lobe is present with traction bronchiectasis (arrows). **E**, Coronal image demonstrates cystic areas (arrows) related to pneumatoceles and varicose and cystic bronchiectasis. **F**, Chest radiograph 4 months after bilateral transplanted lungs with sternal hardware and mediastinal clips. Grossly (**G-K**), the pleural surface of the right lung has adhesions (**G**), whereas that of the left lung (**H**) has few adhesions on the diaphragmatic surface (arrow). The cut surface of the lungs shows consolidation affecting all lobes diffusely (**I**, right lung; **J**, **K**, left lung), with multiple small cysts (arrows, **J**) and bronchiectasis/bronchiolectasis (arrowhead, **J**). The calcified peripheral triangular densities seen on the CT scan (arrowheads, **B**) are seen on the cut surface as denser areas of consolidations (arrows, **K**), with the inset in **K** showing tan white streaks of calcification (arrow).

lobe. The right lower lung regions are severely consolidated with pneumatoceles such as in the right middle lobe and right lower lobe **FIGURE 3B**. The remainder of the lungs is affected by heterogeneous ground-glass opacity such as at the left lung base, which also has consolidation and volume loss **FIGURE 3B**. On chest CT images 2.5 months later, the pneumothorax has resolved, with cysts noted in the right upper lobe. Dense consolidation and ground-glass opacities are present in both upper lobes **FIGURE 3C**. Bilateral cylindrical bronchiectasis has progressed and is now severe in the lower lobes with decreased consolidation, which is decreased, and extensive ground-glass opacity **FIGURE 3D**. A fluid-filled cavity in the right middle lobe is present, adjacent to a cyst **FIGURE 3E**. Mild right pleural thickening is present **FIGURE 3E**. A chest radiograph 3.5 months after transplant demonstrates bilateral surgical changes **FIGURE 3F**.

Gross Findings

The right and left lungs weigh 356.3 and 240.1 g, respectively. The gross findings of the explanted lungs are shown in **FIGURE 3**. The pleural surfaces of the right **FIGURE 3G** and the left **FIGURE 3H** lungs have significant adhesions that could be secondary to the pneumothorax as well as pleural involvement related to multiple secondary bacterial infections. The cut surfaces of the right **FIGURE 3I** and left **FIGURE 3J** lungs show diffuse fibrosis and traction bronchiectasis/bronchiolectasis. The right middle lobe has a cavity with organizing hematoma that corresponds to the fluid-filled cavity seen on CT scans **FIGURE 3E**.

Histologic Findings

The histologic findings in the lungs are shown in **FIGURE 4**. Similar to patient 1, histologically the lung parenchyma shows
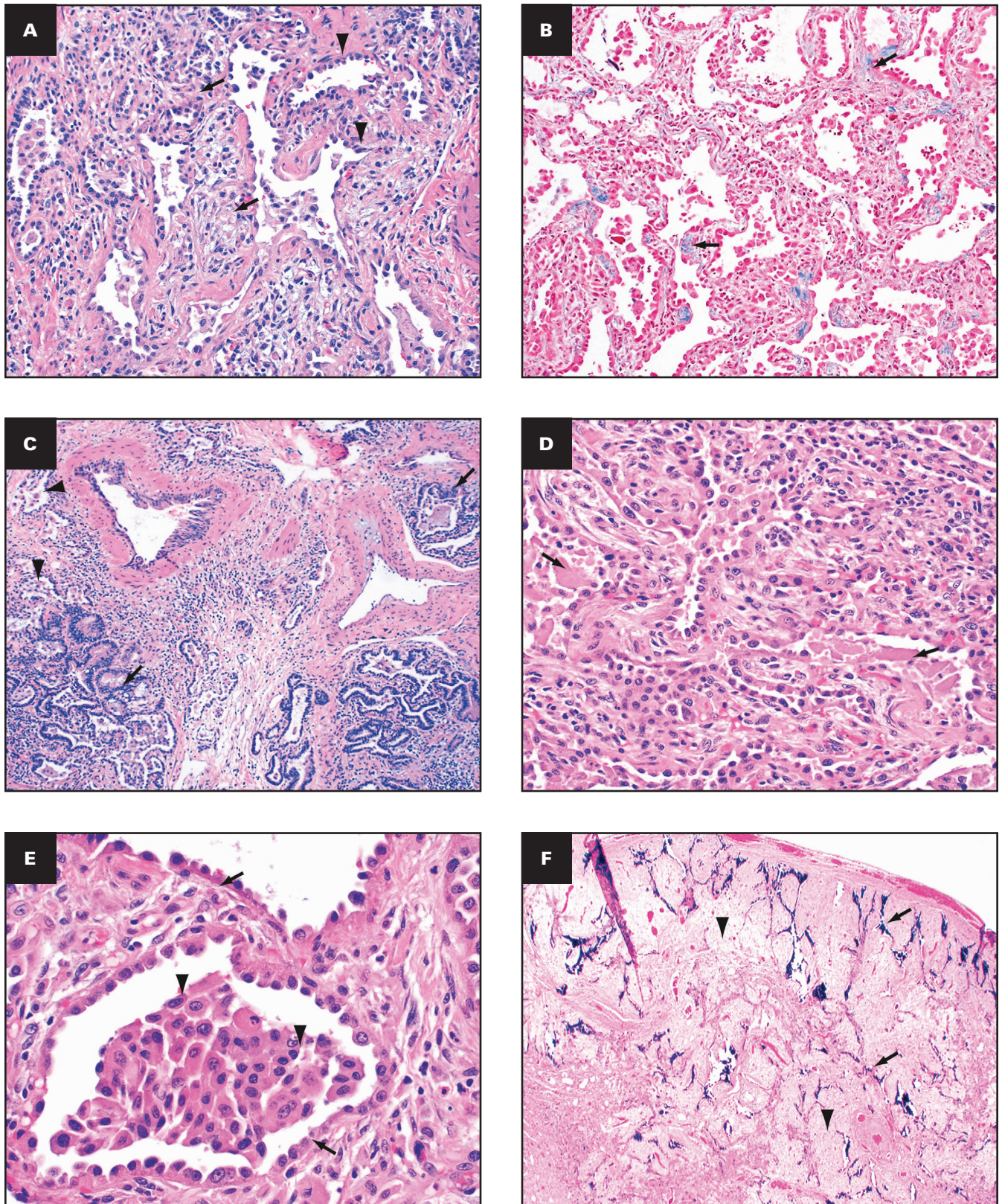
FIGURE 2 Patient 1: Histopathologic findings in lung explant of the 40-year-old woman with coronavirus disease 2019. The lungs show changes of proliferative (**A**) and fibrotic (**B-E**) phases of diffuse alveolar damage. The proliferative phase is characterized by myxoid interstitial fibrosis (arrows, **A**) and reactive type 2 pneumocyte hyperplasia (arrowheads, **A**). The fibrotic phase has varying degrees of fibrosis varying from mild interstitial collagen deposition, as shown on trichrome stain (arrows, **B**), to more marked fibrosis with collapsed alveoli (arrowheads, **C**) and peribronchiolar metaplasia (arrows, **C**). Focal intra-alveolar fibrin is present (arrows, **D**). Diffuse type 2 pneumocyte hyperplasia (arrows, **E**) and macrophages (arrowheads, **E**) is present. The peripheral densities with calcification seen on computed tomography scan and grossly on the cut surface show areas of loose intra-alveolar myxoid fibrosis (arrowheads, **F**) with delicate alveolar septal calcification (arrows, **F**).
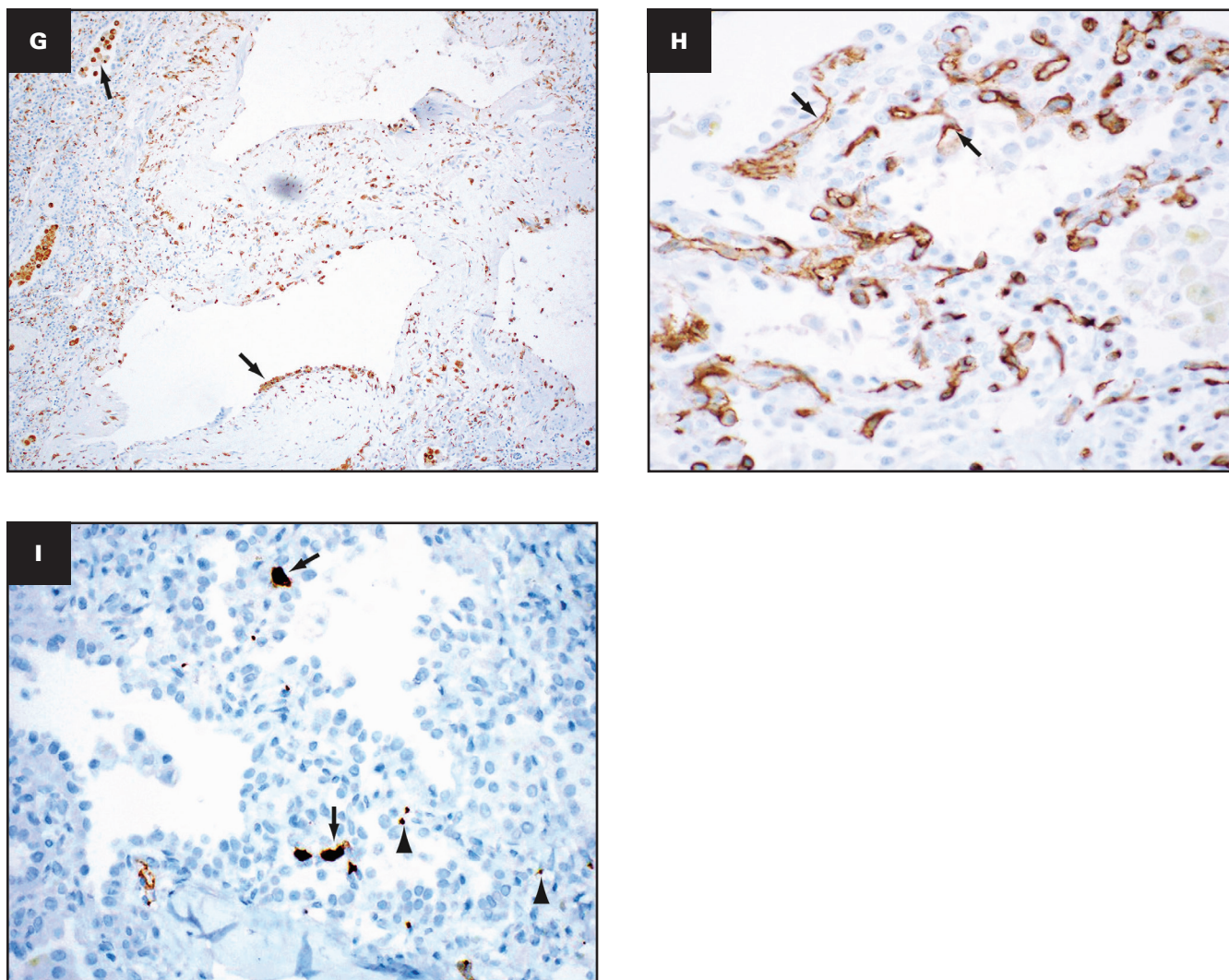
FIGURE 2 (cont) Immunohistochemical stains for CD68 (**G**), CD34 (**H**), and CD61 (**I**) highlight the macrophages (arrows, **G**) lining the pneumatoceles, increased capillaries in the interstitium (arrows, **H**), and platelet microthrombi (arrows, **I**) and platelets (arrowheads, **I**). **A**, **C-E**, H&E; **B**, trichrome; **G**, CD68; **H**, CD34; **I**, CD61. **A**, **D**, ×20; **F**, ×2; **B**, **C**, **G**, ×10; **E**, **H**, **I**, ×40.

overlapping stages of proliferative and fibrotic phases of DAD with prominent type 2 pneumocyte hyperplasia. Honeycomb change is not present. The proliferative phase shows areas of interstitial myxoid fibrosis, and the fibrotic phase shows varying degrees of collagen deposition with preserved architecture FIGURE 4A . Residual compressed alveolar spaces FIGURE 4B with peribronchiolar metaplasia FIGURE 4C are present. In addition to interstitial fibrosis, there is mild to moderate mononuclear inflammation comprising T lymphocytes FIGURE 4D , scattered clusters of B lymphocytes, and intra-alveolar macrophages FIGURE 4E . The larger pulmonary arteries show mild intimal thickening and no evidence of thromboemboli. The medium-sized and small muscular arteries show medial thickening, eccentric intimal thickening, and recanalized thrombi FIGURE 4F , G . Scattered small capillaries with platelet thrombi as well as varying amounts of platelets are present in the lung parenchyma FIGURE 4H . Multiple foci of increased interstitial capillary density are present FIGURE 4I . Both the large cartilaginous and small airways FIGURE 4F show fibrosis of the wall.

Patient 3

Pretransplant Clinical Course

A 47-year-old man TABLE 1 with no medical history was admitted in early April 2020 for severe hypoxemic respiratory failure and ARDS due to COVID-19 pneumonia. He was intubated on hospital day 3 but had refractory hypercapnia and hypoxemia despite deep sedation, paralysis, and prone positioning. Peripheral VV-ECMO was initiated on hospital day 4, and percutaneous tracheostomy was performed on hospital day 5. COVID-19–directed therapies included hydroxychloroquine, azithromycin, glucocorticoids, and clazakizumab. The clinical course was complicated by bilateral pneumothoraces, bronchopleural fistula, alveolar-pleural fistula, and right hemothorax. He also had nosocomial infections,
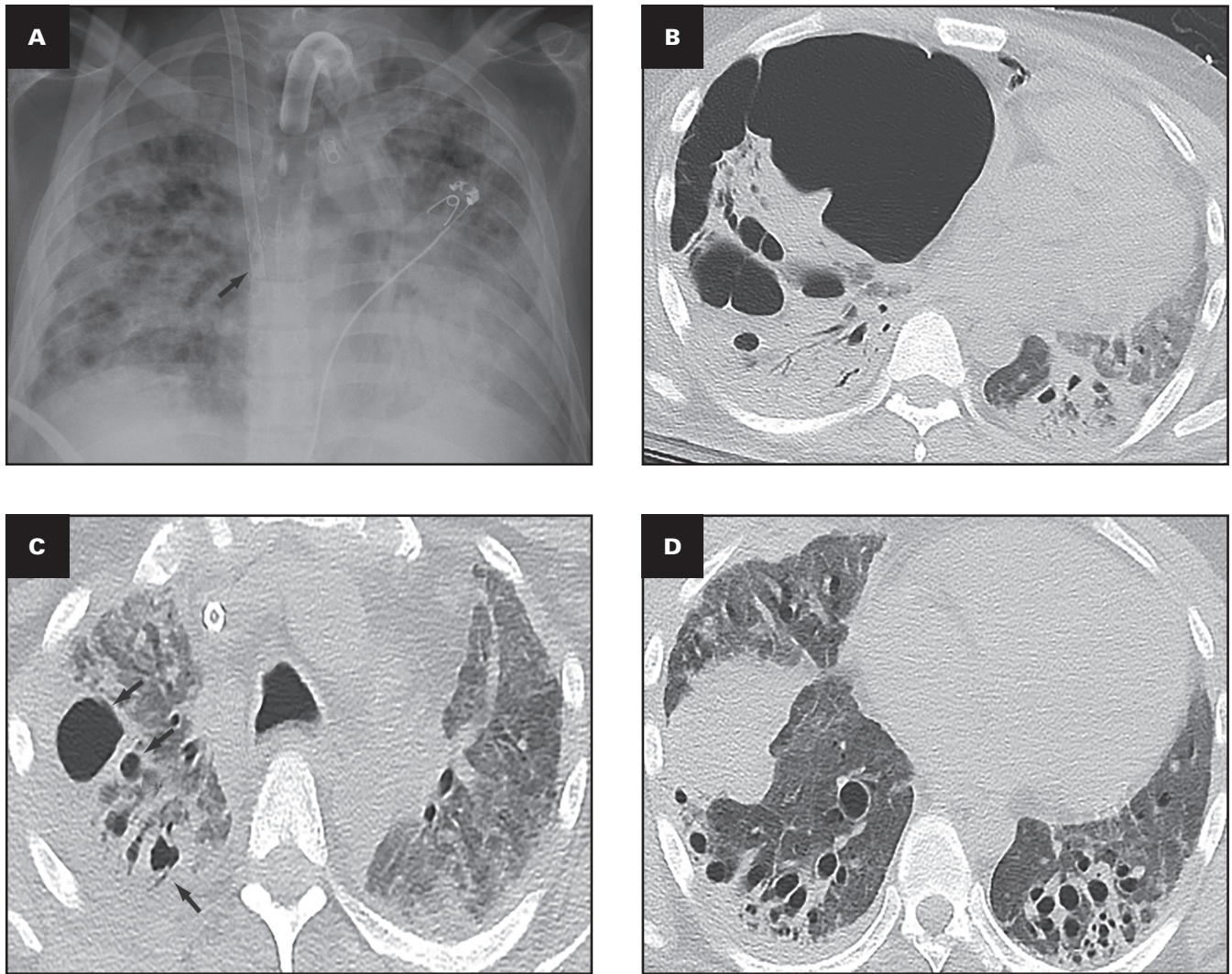
FIGURE 3 Patient 2: A 33-year-old man who had a bilateral lung transplant for coronavirus disease 2019. Overview of radiographic and gross pathologic observations. **A**, Chest radiograph 3 months prior to hospital transfer shows a superior vena cava extracorporeal membrane oxygenation cannula tip overlying the superior cavoatrial junction (arrow), tracheostomy, and severe consolidation. **B**, On an axial lung window image from chest computed tomography (CT) 19 days later, a large right lower hemithorax air collection represents both pneumothorax and cavity. Multiple pneumatoceles (arrow) are in the right lung within bilateral consolidation and diffuse ground-glass attenuation. **C, D**, Two and a half months later, chest CT axial lung window images show opacification of the lung by ground-glass opacities and consolidation with right upper lobe cysts (**C**, arrows). At the lung bases (**D**), cylindrical bronchiectasis is now severe, consolidation is decreased, and extensive ground-glass opacities persist.

including *Pseudomonas aeruginosa*, *Klebsiella pneumoniae*, and *Chryseobacterium indologenes* and *Candida krusei/glabrata* candidemia. He was eventually weaned from VV-ECMO after a total runtime of 135 days; his tracheostomy was decannulated after 176 days. He was discharged from the hospital to acute inpatient rehab after 196 days. The patient was listed for transplant due to his end-stage progressive pulmonary fibrosis. He underwent bilateral lung transplantation 343 days after his index hospitalization for COVID-19 pneumonia. Intraoperatively, both lungs had significant circumferential chest wall adhesions.

Posttransplant Clinical Course
He was extubated on POD 2 and discharged on POD 7. At his 1-month posttransplant follow-up, he is ambulating several city blocks without difficulty and saturating 98% on room air. The patient has not had either recurrence of SARS-CoV-2 infection or allograft rejection following transplant at this time.

Radiologic Findings: Pretransplant and Posttransplant
Representative radiologic findings from this patient and the gross pathologic findings of the explanted lungs are shown in FIGURE 5.

Chest radiograph performed on admission for COVID-19 infection demonstrates patchy dense consolidation bilaterally with a lower lung and mild peripheral predisposition FIGURE 5A. Ten months later, prior to transplantation, chest CT FIGURE 5B , FIGURE 5C , FIGURE 5D , and FIGURE 5E reveals pleural thickening bilaterally, particularly on the right FIGURE 5B . Anteriorly located severe traction bronchiectasis with multiple cysts is seen on axial FIGURE 5E and coronal FIGURE 5C images aligned along a plane FIGURE 5C through the right ventricle. More posterior coronal image FIGURE 5D anterior to
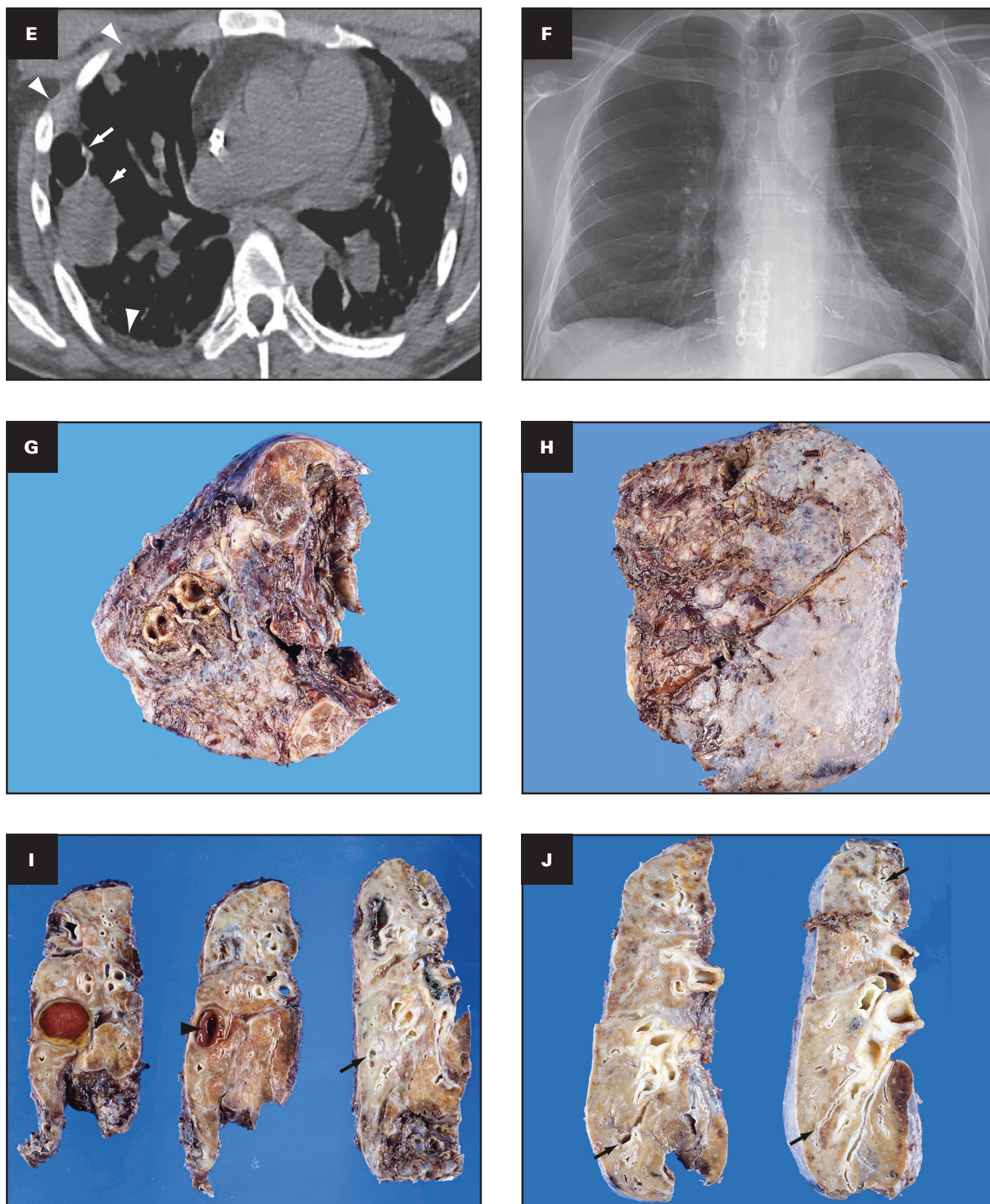
FIGURE 3 (cont) **E**, Axial soft tissue windowed chest CT image shows a cyst (long arrow), fluid-filled cavity in the right middle lobe (short arrow), and right pleural thickening (arrowheads). Some consolidation is evident on the image. **F**, Chest radiograph 3.5 months after transplant demonstrates bilateral lung transplant changes. Grossly (**G-J**), the pleural surfaces of the right (**G**) and left (**H**) lungs have pleural adhesions. The cut surface of the lungs shows consolidation affecting all lobes diffusely (**I**, right lung; **J**, left lung), with bronchiectasis/bronchiolectasis (arrows, **I** and **J**). The right middle lobe has a cavity filled with blood (arrowhead, **I**).
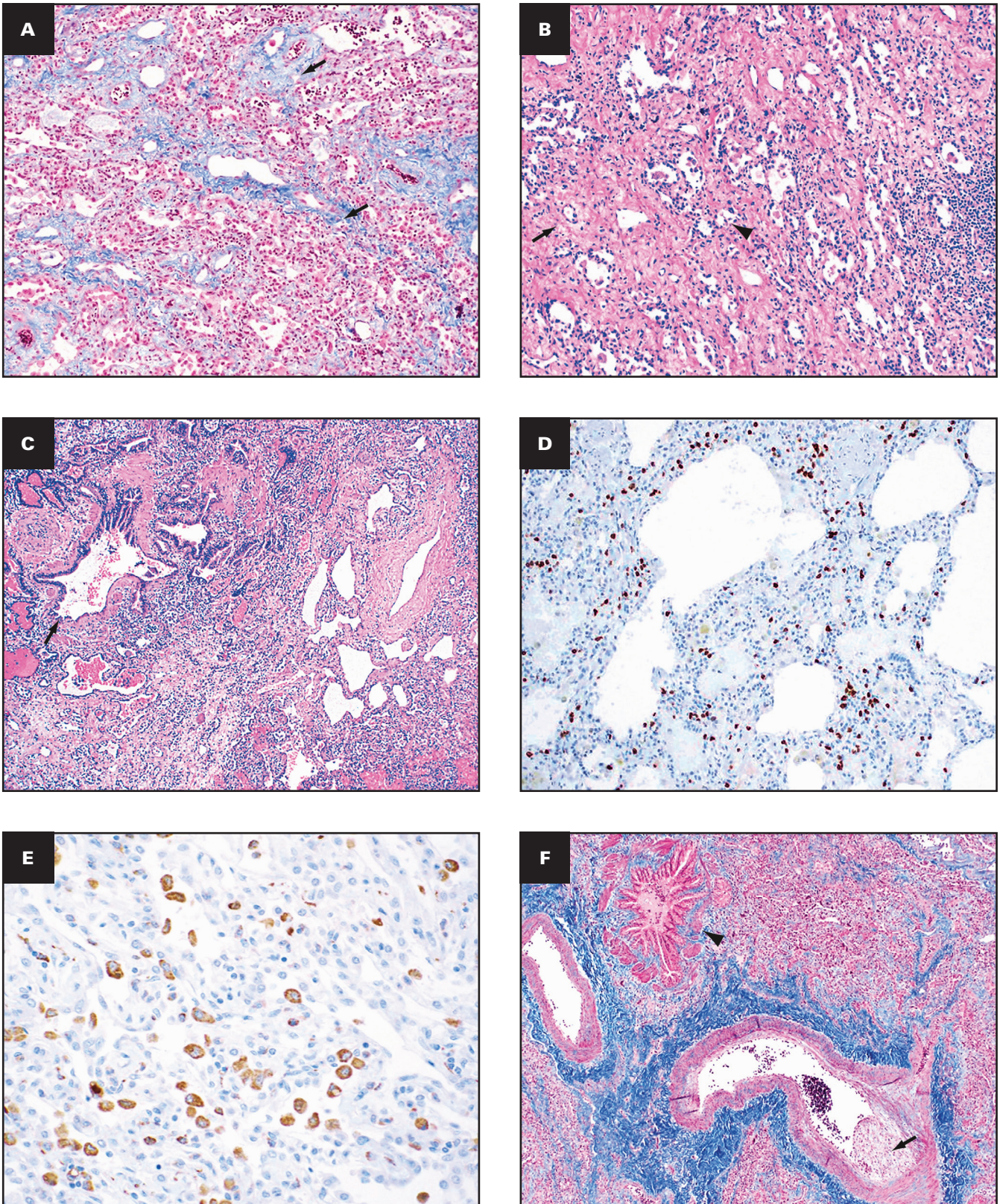
FIGURE 4 Patient 2: Histopathologic findings in lung explant of the 33-year-old man with coronavirus disease 2019. The lungs show interstitial fibrosis varying from mild interstitial fibrosis (arrows, **A**) to more marked fibrosis (arrow, **B**) with collapsed alveoli (arrowhead, **B**). Peribronchiolar metaplasia is present (arrow, **C**). Immunostain for CD3 highlights the interstitial lymphocytic inflammation (**D**) and that for CD68 (**E**) highlights the numerous macrophages. The wall of the small airways has fibrosis (arrowhead, **F**), and the accompanying muscular artery has eccentric intimal fibrosis (arrow, **F**) that likely represents a healed thrombus.
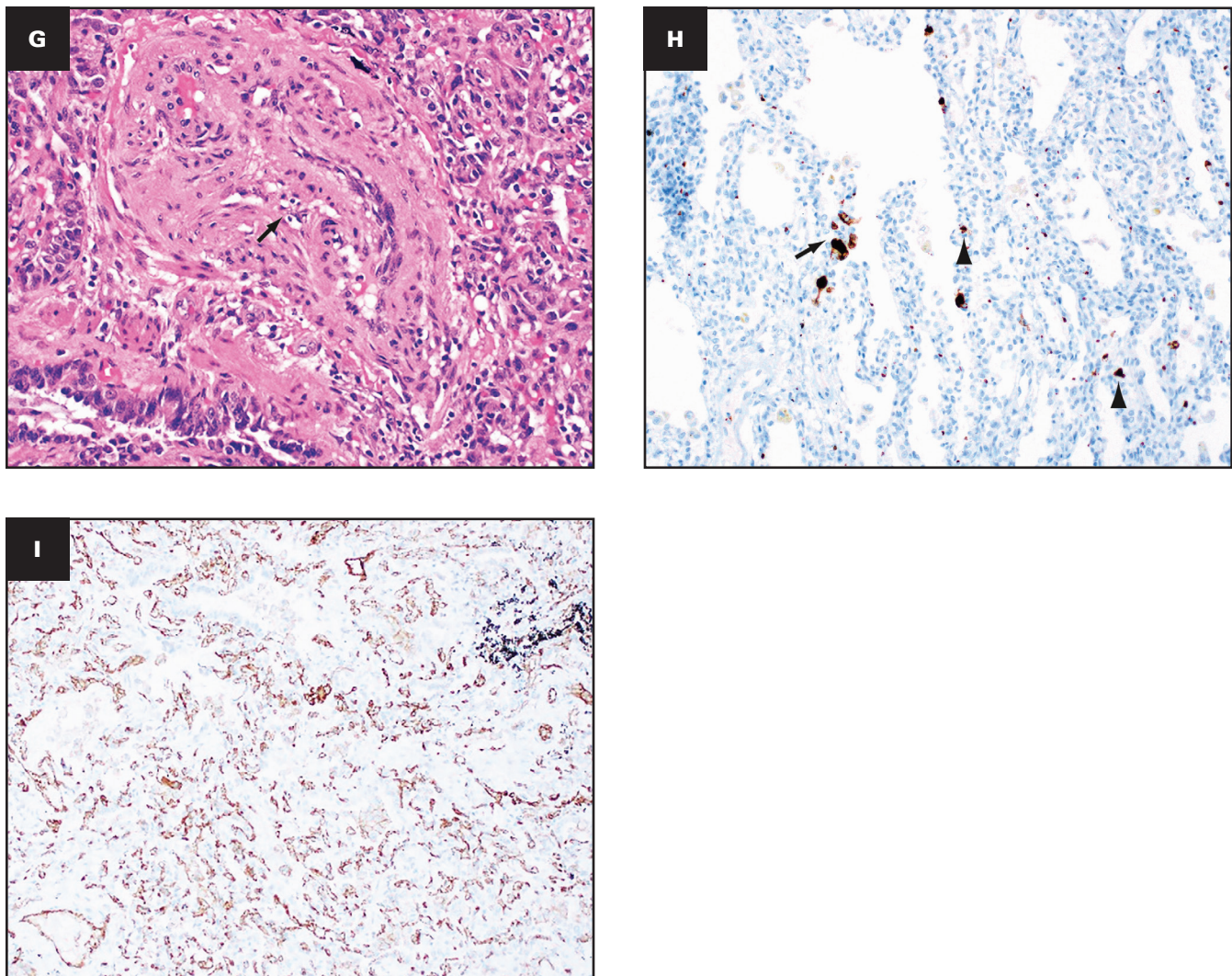
FIGURE 4 (cont) Recanalized thrombus is present in muscular artery (arrow,**G**). Immunostain for CD61 (**H**) shows microvascular thrombi (arrow, **H**) and platelets (arrowheads, **H**) in the parenchyma. Immunostain for CD34 shows increased interstitial capillary density (**I**). **B**, **C**, **G**, H&E; **A**, **F**, trichrome; **E**, CD68; **H**, CD61; **I**, CD34. **A**, **B**, **D**, ×10; **C**, **F**, ×4; **E**, ×40; **G-I**, ×20.

the vertebral bodies shows heterogeneous ground-glass opacities intermixed with bronchial wall thickening, mild cystic areas, and reticular opacities. The parenchymal opacities have a lower lung region predisposition. Chest radiograph 5 weeks after transplant demonstrates small bilateral effusions, mild basilar linear atelectasis, and cardiomegaly **FIGURE 5F** .

Gross Findings

The right and left lungs weigh 741 and 691 g, respectively. The gross findings of the explanted lungs are shown in **FIGURE 5** .The pleural surfaces of the right **FIGURE 5G** and left **FIGURE 5H** lungs have significant adhesions that could be related to the pneumothorax, bronchopleural fistula, and/or multiple secondary bacterial infections. The cut surface of the lungs shows diffuse fibrosis and multiple cysts that represent traction bronchiectasis/bronchiolectasis as well as pneumatoceles **FIGURE 5I** , **FIGURE 5J** , and **FIGURE 5K** . The cystic areas are present more anteriorly in the lungs, and diffuse consolidation is present posteriorly in the right **FIGURE 5J** and left **FIGURE 5L** lungs.

Histologic Findings

The histologic findings in the lungs are shown in **FIGURE 6** . Similar to patients 1 and 2, the lung parenchyma shows overlapping stages of proliferative **FIGURE 6A** and fibrotic **FIGURE 6B** phases of diffuse alveolar damage with prominent type 2 pneumocyte hyperplasia and peribronchiolar metaplasia. Honeycomb change is not present. Varying degrees of interstitial collagen deposition are present with residual compressed alveolar spaces **FIGURE 6C** . Multiple foci of bronchopneumonia with numerous neutrophils, multinucleated giant cells **FIGURE 6D** , ulceration, and squamous metaplasia of the lining of the small airways **FIGURE 6E** are present in this patient. In addition to fibrosis, the lung parenchyma also shows diffuse widening of the alveolar septal wall with mild to moderate mononuclear inflammation comprising T lymphocytes **FIGURE 6F** , clusters of B lymphocytes, and increased interstitial capillary density **FIGURE 6G** . Scattered small capillaries with platelet thrombi as well as varying amounts of platelets are present in the lung parenchyma **FIGURE 6H** . Multiple pneumatoceles lined by macrophages are present **FIGURE 6I** . The large
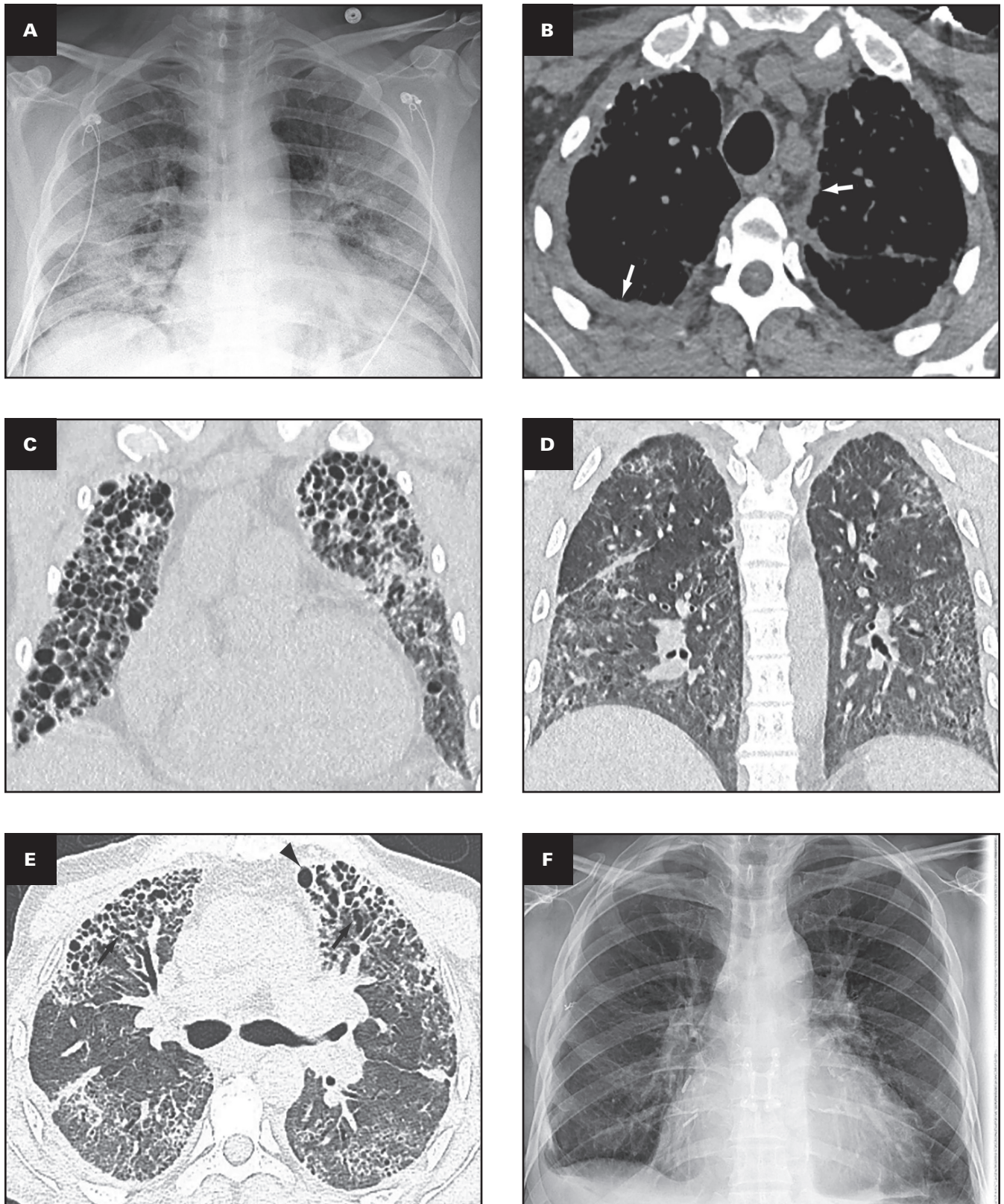
FIGURE 5 Patient 3: A 47-year-old man who had hypoxemic respiratory failure due to coronavirus disease 2019 and underwent bilateral lung transplantation. Overview of radiographic and gross pathologic observations. **A**, Admission chest radiograph with bilateral patchy dense consolidation bilaterally. **B**, Chest computed tomography (CT) soft tissue window image from study 10 months later before transplant with pleural thickening (arrows). **C**, Coronal lung window CT images in a horizontal plane anteriorly through the right ventricle demonstrates numerous cysts from traction bronchiectasis. **D**, Coronal lung window CT images in a horizontal plane posteriorly anterior to the vertebral bodies show ground-glass opacities, reticulation, and mild cystic areas. **E**, Axial lung window image shows the anteriorly located cysts (arrowhead) and connection to bronchiectatic airways (arrows). **F**, Chest radiograph 5 weeks after transplant.
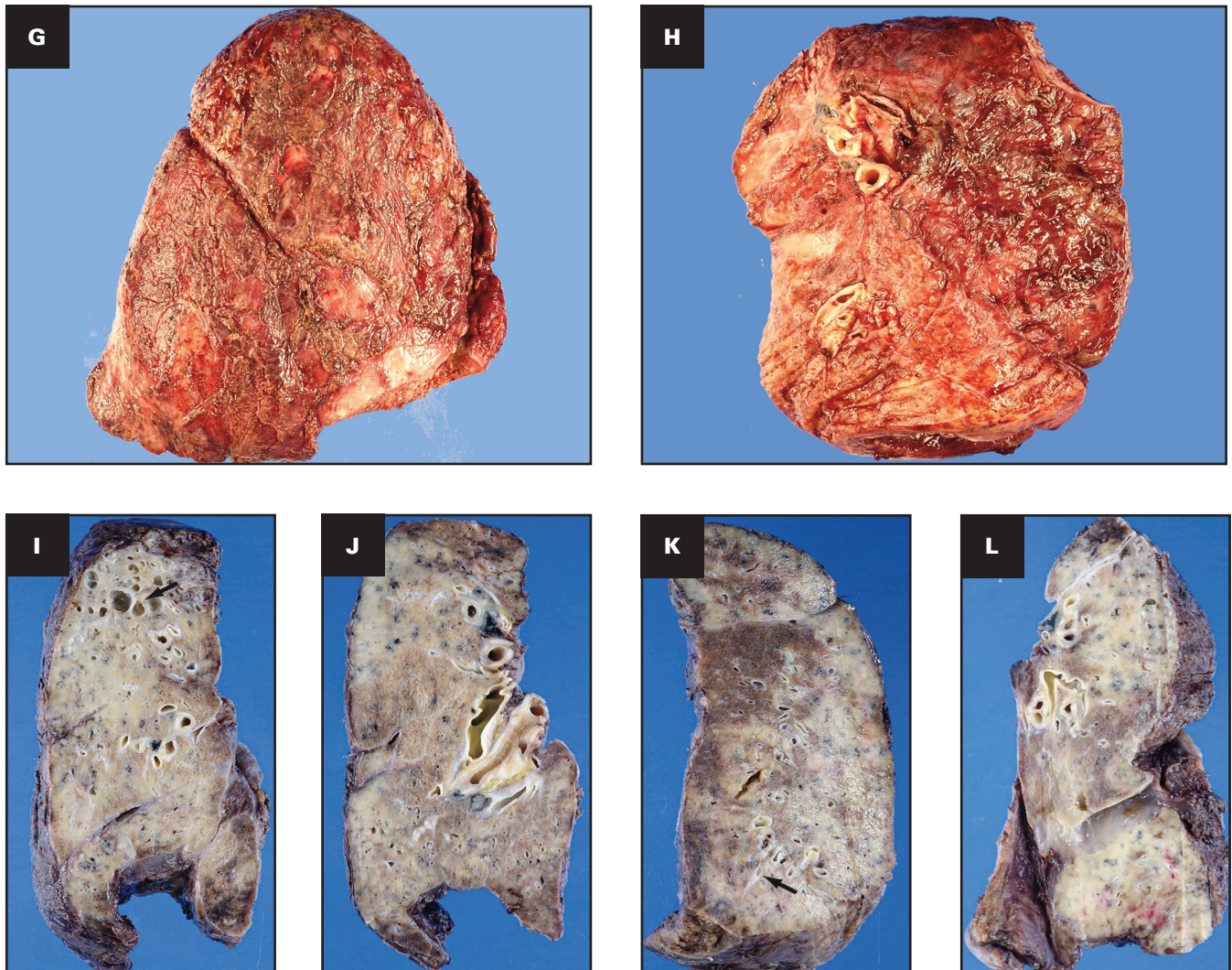
FIGURE 5 (cont) Grossly (**G-L**), the pleural surfaces of the right (**G**) and left (**H**) lungs have pleural adhesions. The cut surface of the lungs shows consolidation affecting all lobes diffusely (**I**, **J**, right lung; **K**, **L**, left lung), with bronchiectasis/bronchiolectasis (arrow, **I** and **K**).

pulmonary arteries show mild intimal thickening, and medial and eccentric intimal hyperplasia is present in the muscular arteries.

SUMMARY OF PATHOLOGIC FEATURES IN LUNG EXPLANTS

Grossly, the pleural surfaces have varying degrees of adhesions. The cut surface of the lungs shows diffuse consolidation involving both upper and lower lobes with cysts. The predominant histologic findings include interstitial fibrosis with bronchiectasis/bronchiolectasis, pneumatoceles, interstitial and intra-alveolar inflammation, and increased interstitial capillary density. The fibrosis varies from established interstitial fibrosis with collagen deposition to interstitial fibroblastic proliferation. Architectural remodeling with honeycomb lung is not seen. The inflammation is composed of T lymphocytes, aggregates of B lymphocytes, and prominent macrophages. Three histologically distinct populations of macrophages are present: foamy macrophages with vacuolated cytoplasm **FIGURE 7A**, hemosiderin-laden macrophages, and macrophages with eosinophilic dense cytoplasm that lack

vacuoles and hemosiderin **FIGURE 7B**. An elastic stain **FIGURE 7C** shows fragmented residual elastic fibers in the interstitium. There is no evidence of vasculitis. Other histologic features include prominent type 2 pneumocyte hyperplasia, peribronchiolar metaplasia, and recanalized thrombi involving small muscular arteries. Large vessel thrombi are not present. Multiplex chromogenic immunohistochemical staining for vimentin, CD34, and CD68 (see method below) shows coexpression of vimentin and CD68 in elongated and spindle-shaped cells with red to orange staining indicative of overlap of the two separate chromogens (arrows in **FIGURE 7D**, **FIGURE 7E**, and **FIGURE 7F**).

METHOD FOR MULTIPLEX CHROMOGENIC IMMUNOHISTOCHEMISTRY

Ready-to-use unconjugated murine anti-human CD34 (cat. 790-2927, RRID: AB_2336013; Ventana Medical Systems) clone QBEnd/10, unconjugated murine anti-human vimentin (cat. 790-2917, RRID: AB_2335925; Ventana Medical Systems) clone V9, and
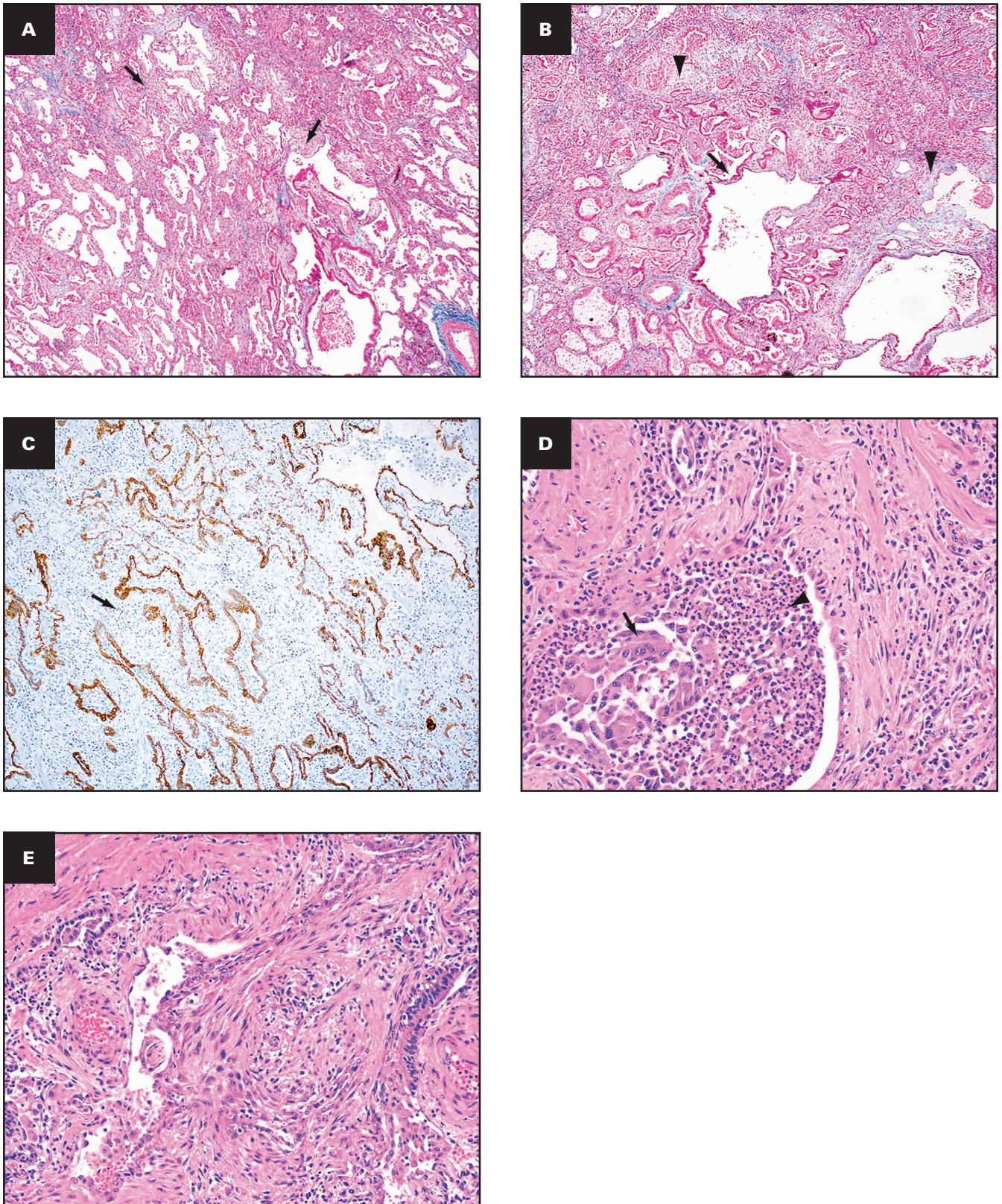
FIGURE 6 Patient 3: Histopathologic findings in the lungs of a 47-year-old man who had hypoxemic respiratory failure due to coronavirus disease 2019 and underwent bilateral lung transplantation. The lungs show features of the proliferative phase of diffuse alveolar damage consisting of myxoid interstitial fibrosis (arrows, **A**). Peribronchiolar metaplasia (arrow, **B**) and interstitial collagen deposition (arrowheads) are present. Immunohistochemical stain for keratin (AE1/3) highlights the widening of the alveolar septa (arrow, **C**). **D**, **E**, Bronchopneumonia with neutrophils (arrowhead) and multinucleated giant cells (arrow) and organizing pneumonia are shown.
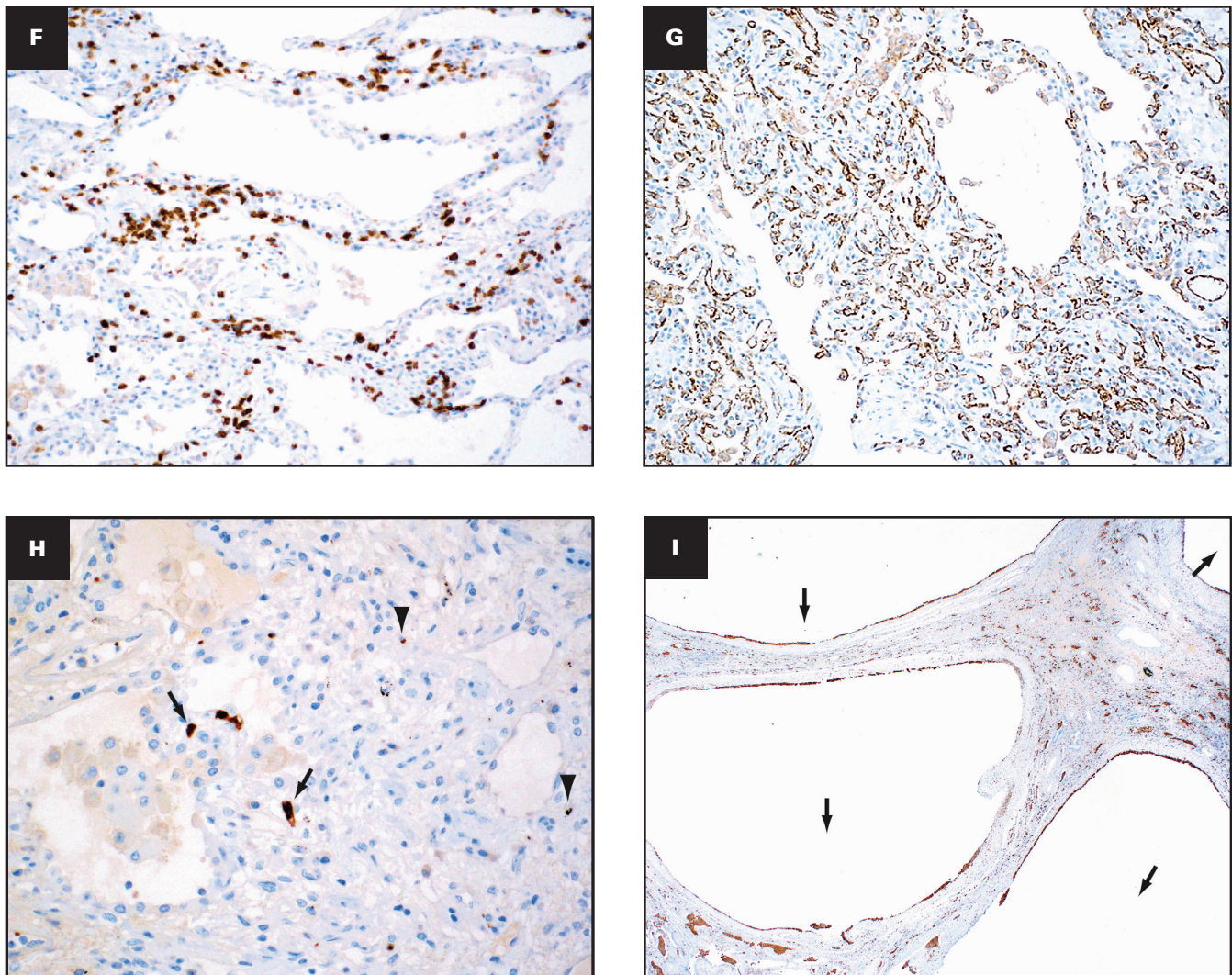
FIGURE 6 (cont) **F**, **G**, Immunohistochemical stains for CD3 and CD31 show the presence of T lymphocytes (**F**) and increased capillary density in the interstitium (**G**). Immunohistochemical stain for CD61 (**H**) shows microvascular thrombi (arrow, **H**) and platelets (arrowheads, **H**) in the parenchyma. Immunohistochemical stain for CD68 shows multiple pneumatoceles (arrows) lined by macrophages (**I**). **A**, **B**, trichrome; **C**, **D**, H&E; **E**, keratin (AE1/3); **F**, CD3; **G**, CD31, **H**, CD61; **I**, CD68. **A**, **B**, ×4; **C**, ×20, **D**, **E**, ×10; **F**, **G**, ×20; **H**; ×40; **I**, ×2.

unconjugated murine anti-human CD68 (cat. 790-2931, RRID: AB_2335972; Ventana Medical Systems) clone KP1 were validated on a Ventana Medical Systems Discovery Ultra platform according to the manufacturer's instructions. Chromogenic-multiplex sequential immunohistochemistry was performed according to best practices.[13] Incubation, antigen retrieval, and application sequence were determined based on antigen retrieval requirements for each marker. Multiplex sequences were iteratively tested with crossover controls to eliminate primary-secondary antibody cross-detection and verify horseradish peroxidase (HRP) quenching. In addition, isotype and diluent (no primary antibody) negative controls were included in the multiplex assay.[14] In brief, endogenous peroxidase was blocked with 3% hydrogen peroxide. CD34 was applied neat, incubated for 30 minutes without antigen retrieval, and detected with goat anti-mouse HRP-conjugated multimer and teal chromogen.[15] Samples were denatured with instrument buffer for 32 minutes. Sections were antigen retrieved using Cell Conditioner

1 (Ventana Medical) (Tris-borate-EDTA pH 8.5) for 24 minutes. Vimentin was applied neat and incubated for 30 minutes, followed by detection with goat anti-mouse HRP-conjugated multimer and magenta chromogen.[15] Samples were denatured with instrument buffer for 32 minutes. CD68 was applied neat and incubated for 30 minutes, followed by detection with goat anti-mouse alkaline phosphatase–conjugated multimer and yellow chromogen.[15] Slides where washed in distilled water, counterstained with hematoxylin, dehydrated through graded alcohols, cleared in xylene, and mounted with synthetic permanent media.

DISCUSSION

The pulmonary pathologic findings seen in these explants are likely multifactorial and could be due to the direct effects of SARS-CoV-2 infection, immune-mediated injury related to severe COVID-19, or secondary bacterial infections, as there was no prior pulmonary
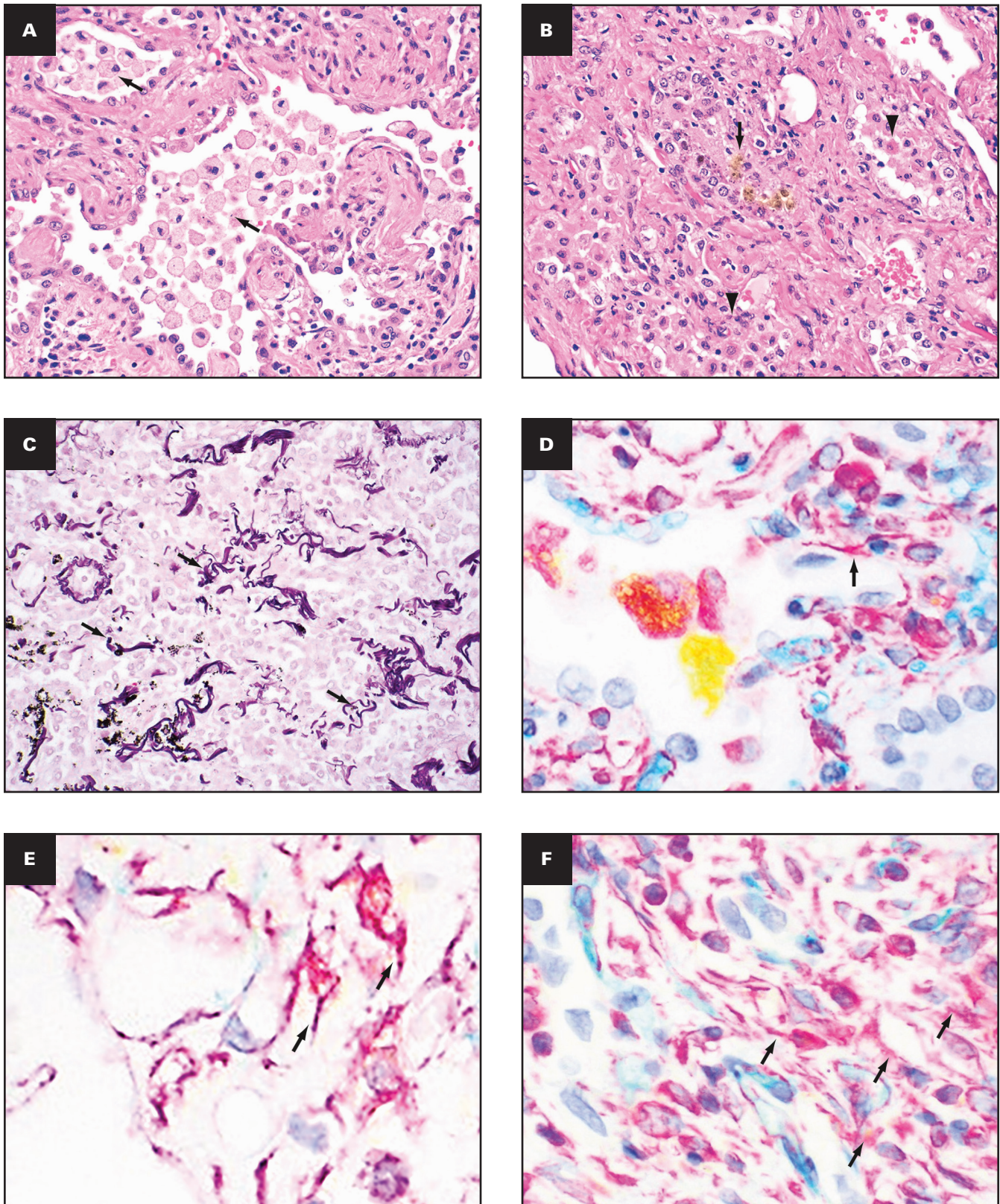
FIGURE 7 Distinct population of macrophages and immunohistochemical evidence suggesting possible transition of macrophages into fibroblast-like cells. Three histologically distinct populations of macrophages are present: foamy macrophages (arrows, **A**) with vacuolated cytoplasm, hemosiderin-laden macrophages (arrow, **B**), and macrophages with eosinophilic dense cytoplasm that lacked vacuoles and hemosiderin (arrowheads, **B**). An elastic stain (**C**) shows fragmented residual elastic fibers in the interstitium (arrows). Multiplex chromogenic immunohistochemical staining for vimentin (magenta) and CD68 (yellow) and CD34 (teal) shows coexpression of vimentin and CD68 in elongated and spindle-shaped cells with red to orange staining (arrows, **D-F**). **A, B**, H&E; **C**, elastic; **D-F**, multiplex immunohistochemical staining for vimentin (magenta), CD68 (yellow), and CD34 (teal). **A-F**, ×40.

disease in these patients.[16-19] The clinical course was complicated by pneumothoraces and culture-proven nosocomial infections in two patients, whereas one patient (patient 1) was treated for presumed bacterial pneumonia. Prior autopsy studies from patients with COVID-19 have reported DAD with hyaline membranes early in the disease course to be the most common underlying pathologic change.[8-12,20,21] The major pathologic findings in the lungs of patients who underwent transplantation 8 to 11 months after SARS-CoV-2 infection included proliferative and fibrotic phases of DAD, diffuse type 2 pneumocyte hyperplasia, prominent interstitial capillary neoangiogenesis, and mononuclear cells, specifically macrophages. The interstitial fibrosis consisted of varying degrees of collagen deposition associated with traction bronchiectasis/ bronchiolectasis with evidence of ongoing injury showing interstitial fibroblastic proliferation; however, architectural remodeling with honeycomb change was not observed. The patients were negative for the virus by PCR testing for several weeks to months before the transplant. Similar to that reported in multi-institutional case series, none of our patients had either recurrence of SARS-CoV-2 infection or allograft dysfunction at this time.[22]

The pattern of interstitial fibrosis was similar to that described by Aesif et al[8] in their case series and resembled nonspecific interstitial pneumonia. All three patients in their series were on prolonged ECMO, whereas only one of our patients was on prolonged ECMO. Similar to patients with non–COVID-19–related ARDS wherein fibrosis has been shown to develop in as early as 1 week,[23] a recent autopsy study has shown that pulmonary fibrosis in SARS-CoV-2 infection starts as early as 15 days from onset of symptoms.[24] The etiology of the ongoing fibrosis could be multifactorial and likely related to the direct and immune-mediated effect of the SARS-CoV-2 infection and also nosocomial infections.[25] Progressive lung fibrosis has been shown to develop in a mouse model after infection with *Streptococcus pneumoniae* by releasing cytotoxic factors that promote apoptosis of epithelial cells and subsequent fibrosis.[19]

After lung injury, type 2 pneumocytes self-renew and give rise to type 1 pneumocytes. Failure to do so could result in fibroblastic proliferation by epithelial-mesenchymal transition.[26,27] Latent viral infections such as that seen with γherpesvirus infection that persists in epithelial cells has been shown to augment lung fibrosis in murine models by increasing production of profibrotic factors such as TGF-β1.[28] Cytology samples of olfactory epithelium from patients with long-term persistence of anosmia after COVID-19 showed the presence of SARS-CoV-2 virus transcripts with associated inflammation.[29] The presence of ongoing injury with diffuse type 2 pneumocyte hyperplasia and myxoid fibrosis in the lung explants months after the initial infection may in part reflect ongoing lung injury related to persistence of the SARS-CoV-2 virus. Persistent stem cell activation due to prolonged inflammatory states and infection leads to stem cell exhaustion. This can drive abnormal repair and failure of alveolar regeneration and is associated with aberrant expression of transforming growth factor–β (TGF-β), Wnt/β-catenin, and sonic hedgehog signaling pathways.[30-34]

Notably, lungs from patients with COVID-19 showed increased RNA expression of TGFBR2 compared with lungs of patients with influenza A (H1N1).[35] TGFBR2 is important in the TGF-β signaling pathway and plays an important role in pulmonary fibrosis by fibroblast activation and myofibroblast proliferation.[36] Currently, the evidence base for the use of antifibrotics in diffuse alveolar damage is limited. We also note that there are phase II to IV trials under way evaluating the potential for repurposing antifibrotic agents in the setting of COVID-19.[37] In a case series of three patients, the combination of pirfenidone, azithromycin, and prednisolone in post-H1N1 ARDS fibrosis showed clinical and radiologic improvement.[38]

Different types of macrophages in the explanted lungs reflect the underlying pathogenesis. Foamy macrophages with fine vacuoles are seen in postobstructive pneumonia and have been described in patients with COVID-19 secondary to small airway obstruction.[8] Hemosiderin-laden macrophages are seen in patients with prior hemorrhage. Although no vasculitis or capillaritis is seen in the lungs, the pathologic change is similar to that described in the proliferative and fibrotic phase of diffuse alveolar damage in which there is injury to the alveolar capillary membrane with resultant hemosiderin-laden macrophages.[39] A third population of macrophages with eosinophilic cytoplasm that lacks vacuoles and hemosiderin is present. Previous studies have reported that late cases of COVID-19 have a macrophage-rich inflammatory component. It has been shown that, in the later stages of COVID-19, macrophages could contribute to fibrosis as they interact with the fibroblasts in the alveolar wall.[40] While M1 macrophages are predominant in the acute phase of acute lung injury (ALI) and have a proinflammatory function, M2 macrophages are involved in the resolving phase of ALI and have been shown to play a role in the development of lung fibrosis via cytokine pathways.[41] Antifibrotic drugs such as pirfenidone mainly target the TGF-β pathway, but they have also been shown to suppress the activity of pulmonary fibroblasts by reducing the M2 macrophages.[42] In a mouse model of lipopolysaccharide-induced ALI, pirfenidone has been shown to reduce both inflammation and fibrosis by blocking the activation of the NLRP3 inflammasome.[43] Transition of macrophages into fibroblast-like cells has been reported after myocardial infarction and during renal fibrosis.[44,45] The combined presence of spindle cell morphology with coexpression of macrophage (CD68) and mesenchymal (vimentin) markers, although speculative as vimentin is not a specific marker for fibroblasts, suggests that macrophages may transition into fibroblast-like cells. However, additional studies are needed to resolve this potential mechanism as being one of the pathways.

A prominent and consistent feature seen in end-stage lungs due to SARS-CoV-2 is the presence of multiple foci of increased interstitial capillary density with occasional foci of microvascular thrombosis, megakaryocytes, and platelets in the lung parenchyma. An autopsy study comparing the morphologic differences between lungs of patients who died of ARDS due to SARS-CoV-2 and those who died of H1N1 infection showed that lungs from patients with

COVID-19 had characteristic intussusceptive or nonsprouting angiogenesis by scanning electron microscopy as well as widespread vascular thrombosis with endothelial injury.[10] Similar findings, referred to as vascular congestion and hemangiomatosis-like change (VCHL), were seen in 50% of cases in another series. Interestingly, there was a negative correlation between the presence of ALI and VCHL.[11]

None of our patients had evidence of thrombosis in the larger branches of the elastic pulmonary arteries. However, despite their being on anticoagulants, the presence of persistent thrombosis in the microvasculature and recanalized thrombi in the small and medium muscular arteries emphasizes the importance of appropriate and continued thromboprophylaxis even months after the infection. The specificity of vascular thrombi in end-stage COVID-19 lungs is unclear as, based on our personal observations (unpublished observation), explanted lungs with end-stage fibrosis from other etiologies, including pulmonary hypertension, also show microvascular thrombi in addition to increased megakaryocytes and platelets in the lung parenchyma.

CONCLUSIONS

The major pathologic findings in the lung explants of patients with SARS-CoV-2 infection suggest ongoing fibrosis, inflammation, and persistent microvascular thrombosis. Characterization of pathologic findings could help develop novel management strategies.

REFERENCES

1. Richardson S, Hirsch JS, Narasimhan M, et al; the Northwell COVID-19 Research Consortium. Presenting characteristics, comorbidities, and outcomes among 5700 patients hospitalized with COVID-19 in the New York City area. *JAMA.* 2020;323:2052-2059.

2. Beigel JH, Tomashek KM, Dodd LE. Remdesivir for the treatment of Covid-19—preliminary report. Reply. *N Engl J Med.* 2020;383:994.

3. RECOVERY Collaborative Group, Horby P, Lim WS, et al. Dexamethasone in hospitalized patients with Covid-19. *N Engl J Med.* 2021;384:693-704.

4. van der Mark SC, Hoek RAS, Hellemons ME. Developments in lung transplantation over the past decade. *Eur Respir Rev.* 2020;29:190132.

5. Bharat A, Querrey M, Markov NS, et al. Lung transplantation for patients with severe COVID-19. *Sci Transl Med.* 2020;12:eabe4282.

6. Chen JY, Qiao K, Liu F, et al. Lung transplantation as therapeutic option in acute respiratory distress syndrome for coronavirus disease 2019–related pulmonary fibrosis. *Chin Med J (Engl).* 2020;133:1390-1396.

7. Cypel M, Keshavjee S. When to consider lung transplantation for COVID-19. *Lancet Respir Med.* 2020;8:944-946.

8. Aesif SW, Bribriesco AC, Yadav R, et al. Pulmonary pathology of COVID-19 following 8 weeks to 4 months of severe disease: a report of three cases, including one with bilateral lung transplantation. *Am J Clin Pathol.* 2021;155:506-514.

9. Arrossi AV, Farver C. The pulmonary pathology of COVID-19 [published online September 23, 2020]. *Cleve Clin J Med.*

10. Ackermann M, Mentzer SJ, Jonigk D. Pulmonary vascular pathology in Covid-19: reply. *N Engl J Med.* 2020;383:888-889.

11. De Michele S, Sun Y, Yilmaz MM, et al. Forty postmortem examinations in COVID-19 patients. *Am J Clin Pathol.* 2020;154:748-760.

12. Borczuk AC, Salvatore SP, Seshan SV, et al. COVID-19 pulmonary pathology: a multi-institutional autopsy cohort from Italy and New York City. *Mod Pathol.* 2020;33:2156-2168.

13. Taube JM, Akturk G, Angelo M, et al. The Society for Immunotherapy in Cancer statement on best practices for multiplex immunohistochemistry (IHC) and immunofluorescence (IF) staining and validation. *J Immunother Cancer.* 2020;8:e000155.

14. Cenaj O, Allison DHR, Imam R, et al. Evidence for continuity of interstitial spaces across tissue and organ boundaries in humans. *Commun Biol.* 2021;4:436.

15. Day WA, Lefever MR, Ochs RL, et al. Covalently deposited dyes: a new chromogen paradigm that facilitates analysis of multiple biomarkers in situ. *Lab Invest.* 2017;97:104-113.

16. Melms JC, Biermann J, Huang H, et al. Author correction: a molecular single-cell lung atlas of lethal COVID-19. *Nature.* 2021;598:E2.

17. Rendeiro AF, Casano J, Vorkas CK, et al. Profiling of immune dysfunction in COVID-19 patients allows early prediction of disease progression. *Life Sci Alliance.* 2021;4:e202000955.

18. Rendeiro AF, Ravichandran H, Bram Y, et al. The spatial landscape of lung pathology during COVID-19 progression. *Nature.* 2021;593:564-569.

19. Knippenberg S, Ueberberg B, Maus R, et al. *Streptococcus pneumoniae* triggers progression of pulmonary fibrosis through pneumolysin. *Thorax.* 2015;70:636-646.

20. Batah SS, Fabro AT. Pulmonary pathology of ARDS in COVID-19: a pathological review for clinicians. *Respir Med.* 2021;176:106239.

21. Borczuk AC. Pulmonary pathology of COVID-19: a review of autopsy studies. *Curr Opin Pulm Med.* 2021;27:184-192.

22. Bharat A, Machuca TN, Querrey M, et al. Early outcomes after lung transplantation for severe COVID-19: a series of the first consecutive cases from four countries. *Lancet Respir Med.* 2021;9:487-497.

23. Vasarmidi E, Tsitoura E, Spandidos DA, et al. Pulmonary fibrosis in the aftermath of the COVID-19 era (review). *Exp Ther Med.* 2020;20:2557-2560.

24. Yao XH, Luo T, Shi Y, et al. A cohort autopsy study defines COVID-19 systemic pathogenesis. *Cell Res.* 2021;31:836-846.

25. Fàbregas N, Torres A, El-Ebiary M, et al. Histopathologic and microbiologic aspects of ventilator-associated pneumonia. *Anesthesiology.* 1996;84:760-771.

26. Barkauskas CE, Noble PW. Cellular mechanisms of tissue fibrosis: 7. New insights into the cellular mechanisms of pulmonary fibrosis. *Am J Physiol Cell Physiol.* 2014;306:C987-C996.

27. Salton F, Volpe MC, Confalonieri M. Epithelial-mesenchymal transition in the pathogenesis of idiopathic pulmonary fibrosis. *Medicina (Kaunas).* 2019;55:83.

28. Vannella KM, Luckhardt TR, Wilke CA, et al. Latent herpesvirus infection augments experimental pulmonary fibrosis. *Am J Respir Crit Care Med.* 2010;181:465-477.

29. de Melo GD, Lazarini F, Levallois S, et al. COVID-19-related anosmia is associated with viral persistence and inflammation in human olfactory epithelium and brain infection in hamsters. *Sci Transl Med.* 2021;13:eabf8396.

30. Pain M, Bermudez O, Lacoste P, et al. Tissue remodelling in chronic bronchial diseases: from the epithelial to mesenchymal phenotype. *Eur Respir Rev.* 2014;23:118-130.

31. Chilosi M, Poletti V, Zamò A, et al. Aberrant Wnt/beta-catenin pathway activation in idiopathic pulmonary fibrosis. *Am J Pathol.* 2003;162:1495-1502.

32. Mora AL, Rojas M. Adult stem cells for chronic lung diseases. *Respirology.* 2013;18:1041-1046.

33. Harrell CR, Sadikot R, Pascual J, et al. Mesenchymal stem cell-based therapy of inflammatory lung diseases: current understanding and future perspectives. *Stem Cells Int.* 2019;2019:4236973.

34. Li J, Wang X, Li N, et al. Feasibility of mesenchymal stem cell therapy for COVID-19: a mini review. *Curr Gene Ther.* 2020;20:285-288.

35. Ackermann M, Verleden SE, Kuehnel M, et al. Pulmonary vascular endothelialitis, thrombosis, and angiogenesis in Covid-19. *N Engl J Med.* 2020;383:120-128.

36. Liang C, Li X, Zhang L, et al. The anti-fibrotic effects of microRNA-153 by targeting TGFBR-2 in pulmonary fibrosis. *Exp Mol Pathol.* 2015;99:279-285.

37. Yim J, Lim HH, Kwon Y. COVID-19 and pulmonary fibrosis: therapeutics in clinical trials, repurposing, and potential development. *Arch Pharm Res.* 2021;44:499-513.

38. Saha A, Vaidya PJ, Chavan VB, et al. Combined pirfenidone, azithromycin and prednisolone in post-H1N1 ARDS pulmonary fibrosis. *Sarcoidosis Vasc Diffuse Lung Dis.* 2018;35:85-90.

39. Tomashefski JF Jr. Pulmonary pathology of acute respiratory distress syndrome. *Clin Chest Med.* 2000;21:435-466.

40. Rendeiro AF, Ravichandran H, Bram Y, et al. The spatial landscape of lung pathology during COVID-19 progression. *Nature.* 2021;593:564-569.

41. Johnston LK, Rims CR, Gill SE, et al. Pulmonary macrophage subpopulations in the induction and resolution of acute lung injury. *Am J Respir Cell Mol Biol.* 2012;47:417-426.

42. Toda M, Mizuguchi S, Minamiyama Y, et al. Pirfenidone suppresses polarization to M2 phenotype macrophages and the fibrogenic activity of rat lung fibroblasts. *J Clin Biochem Nutr.* 2018;63:58-65.

43. Li Y, Li H, Liu S, et al. Pirfenidone ameliorates lipopolysaccharide-induced pulmonary inflammation and fibrosis by blocking NLRP3 inflammasome activation. *Mol Immunol.* 2018;99:134-144.

44. Haider N, Boscá L, Zandbergen HR, et al. Transition of macrophages to fibroblast-like cells in healing myocardial infarction. *J Am Coll Cardiol.* 2019;74:3124-3135.

45. Meng XM, Wang S, Huang XR, et al. Inflammatory macrophages can transdifferentiate into myofibroblasts during renal fibrosis. *Cell Death Dis.* 2016;7:e2495.